Reconstruction simultanée des propriétés optiques de tissus biologiques par la tomographie photoacoustique quantitative

F. Asllanaj[1], A. Addoum[2]
[1] : *LEMTA (CNRS UMR 7563), université de Lorraine F-54504, Nancy, France*
[2] : *Institut de Physique des 2 Infinis de Lyon (IP2I UMR 5822), Université de Claude Bernard Lyon 1, F-69622, Lyon, France*
Email : Fatmir.Asllanaj@univ-lorraine.fr

Résumé

Ce travail présente pour la première fois la reconstruction simultanée des propriétés optiques de tissus biologiques à savoir les coefficients d'absorption μ_a et de diffusion μ_s ainsi que le facteur d'anisotropie g de la fonction de phase de Henyey-Greenstein. La propagation de la lumière est modélisée par l'équation de transfert radiatif. La reconstruction est basée sur une méthode d'optimisation non-linéaire de type-gradient. Les images 2D obtenues montrent que notre algorithme est en mesure de reconstruire simultanément les propriétés optiques, avec une bonne précision, même en présence de bruit de mesure.

1. Introduction

La Tomographie photoacoustique quantitative (QPAT) est une technique d'imagerie non-invasive qui consiste à éclairer le tissu par une source Laser pulsée et à estimer les propriétés optiques en utilisant la distribution de l'énergie lumineuse absorbée dans le milieu [1-2-3]. L'effet photoacoustique se réfère aux ondes acoustiques générées suite à l'absorption de la lumière dans le tissu. Dans la littérature, la reconstruction simultanée de μ_a et μ_s a été suffisamment étudié en utilisant l'imagerie optique alors que, la reconstruction simultanée de trois paramètres n'a pas encore été étudiée à notre connaissance. Néanmoins, il a été montré que le facteur g peut être un contraste endogène pour marquer les tumeurs cancéreuses [4].

2. Modèles direct et inverse

L'équation de transfert radiatif (ETR) modélise rigoureusement la propagation de la lumière dans le tissu. En régime stationnaire, elle est donnée par :

$$\left[\boldsymbol{\Omega}\cdot\nabla+\left(\mu_a(\boldsymbol{r})+\mu_s(\boldsymbol{r})\right)\right]\psi_s(\boldsymbol{r},\boldsymbol{\Omega})-\mu_s(\boldsymbol{r})\int_{\Omega'=2\pi}p(\boldsymbol{\Omega'}\cdot\boldsymbol{\Omega})\,\psi_s(\boldsymbol{r},\boldsymbol{\Omega'})\,\mathrm{d}\Omega'-S_c(\boldsymbol{r},\boldsymbol{\Omega})=0$$

où ψ_s est la luminance diffuse et S_c est le terme source lié à la luminance collimatée ψ_c. p représente la fonction de phase de Henyey-Greenstein où intervient le paramètre g [4]. La densité d'énergie absorbée dans le tissu est donnée par :

$$A(\boldsymbol{r})=\mu_a(\boldsymbol{r})\,\psi_c(\boldsymbol{r})+\mu_a(\boldsymbol{r})\Phi_s(\boldsymbol{r})\quad\text{avec}\quad\Phi_s(\boldsymbol{r})=\int_{\Omega=2\pi}\psi_s(\boldsymbol{r})\,\mathrm{d}\Omega$$

Le problème inverse en QPAT est résolu par une méthode d'optimisation non-linéaire de descente de gradient. Le calcul de ce dernier constitue une étape importante pour la reconstruction notamment lorsque le nombre de paramètres à reconstruire est élevé (plusieurs milliers d'inconnus). Nous avons utilisé la méthode adjointe pour déterminer le gradient de la fonction objective ainsi que la direction Lm-BFGS de Quasi-Newton afin d'ajuster le vecteur des paramètres optiques [4].

3. Résultats

Le fantôme numérique est un carré de longueur 1 cm. Il contient deux inclusions circulaires de rayon 1 mm centrées à (2 mm; 2 mm) et (-2 mm; -2 mm) dont les valeurs optiques sont respectivement égales à μ_a = 0.06 mm^{-1}, μ_s = 6 mm^{-1} et g = 0.85 et μ_a = 0.04 mm^{-1}, μ_s = 4 mm^{-1} et g = 0.95. Ces inclusions sont insérées dans un fond homogène avec μ_a = 0.05 mm^{-1}, μ_s = 5 mm^{-1} et g = 0.9. Ces valeurs sont utilisées pour l'initialisation du problème inverse. Quatre sources Laser Gaussienne avec un FWHM de 2 mm éclairent chacune des faces du fantôme. Un bruit de mesure de 6 % est considéré. Les résultats sont illustrés dans la Figure 1.

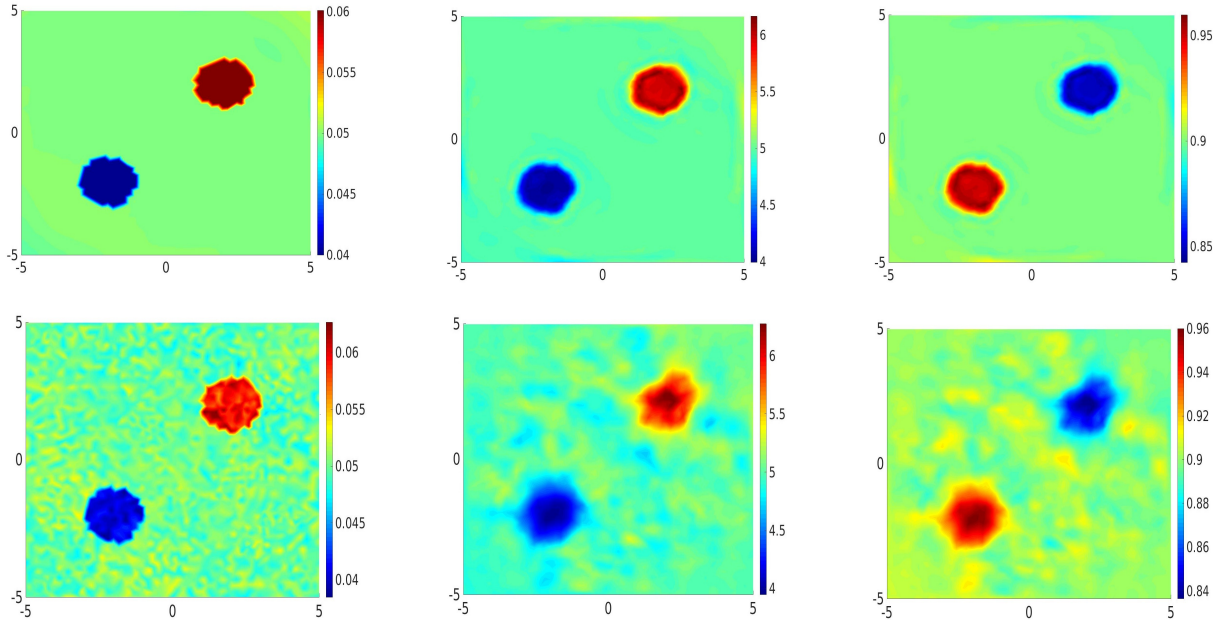

Figure 1 : La reconstruction simultanée de μ_a (colonne de gauche), μ_s (colonne centrée) et g (colonne de droite) sans bruit de mesure (première ligne) et avec 6% de bruit (deuxième ligne)

La figure montre que la qualité des images se dégrade lorsque les mesures sont bruitées. En revanche, notre algorithme d'inversion a réussi à localiser correctement les inclusions dans leurs positions exactes même en présence de bruit de mesure. Quantitativement, il a retrouvé avec une bonne précision les valeurs de μ_a, μ_s et g avec une légère sous ou sur estimation par rapport à leurs valeurs exactes.

4. Conclusion

Ces résultats reportent pour la première fois la reconstruction simultanée des trois propriétés optiques de tissus biologiques à savoir μ_a, μ_s et g en utilisant l'imagerie photoacoustique quantitative. L'intérêt de cette dernière est qu'elle permettra d'éviter d'introduire des informations à priori pour la caractérisation optique des tumeurs lors des études précliniques. Ceci rend alors la QPAT supérieure à l'imagerie optique qui exploite uniquement la lumière diffuse.

6. Bibliographie

[1] Wang LV and Hu S 2012 Photoacoustic tomography: in vivo imaging from organelles to organs *Science*, 335(6075), 1458-1462.

[2] Cox B, Laufer JG, Arridge SR and Beard PC 2012 Quantitative spectroscopic photoacoustic imaging: a review, *J. Biomed. Optics*, 17(6), 061202.

[3] Wang LV, Photoacoustic imaging and spectroscopy, CRC Press, Florida, 2009.

[4] Addoum A, Contassot-Vivier S and Asllanaj F, Three-dimensional frequency-domain optical anisotropy imaging of biological tissues with near-infrared light, *J. Med. Phys.*, 2019, https://doi.org/10.1002/mp.13636.

Photonic crystal textile in the Mid InfraRed for thermoregulation

S. Assaf, M. Boutghatin, Y. Pennec, V. Thomy, M. Carette, B.Djafari-Rouhani
IEMN, Université Lille, Villeneuve d'Ascq, France
Salim.alhajj-assaf@univ-lille.fr

Résumé
The effect of a photonic polymer membrane in the Mid Infrared (MIR) range for passive personal heating regulation is demonstrated. We show that by designing the holes' diameters and periods of the membrane, we are able to the transmission amplitude by 28% in benefit of both absorption and reflection in the wavelength range [7.5, 11.5] µm. The work presented here has been performed theoretically with the help of the Finite Element Method. And then we have devoted to studying analytically the thermal properties of BCB polymer membranes. Integrated to a textile, such a membrane can greatly mitigate the energy demand for indoor heating and ultimately contributes to the relief of the climate issues.

1. Introduction

A large part of the building energy consumption is attributed to temperature control using Heating, Ventilation and Air Conditioning (HVAC) systems [1]. A decrease in this consumption, even slightly, will contribute to both environmental protection and costs saving. One way is to support building insulation; another way is to control the energy consumption by personal thermoregulation [2]. Toward this end, personal thermoregulation properties have been recently developed, not only in extreme environments for military personnel, athletes or emergency medical service personnel [3], but for the majority of people who spend their time in a sedentary state. The personal thermal management has been defined through different devices, wearable like normal clothes, but capable to control the body comfort. Personal cooling textile have been developed using synthetic polymer fibers with low IR absorbance [4][5] or able to enhance the radiative dissipation by nonporous polyethylene film [6].

For the past ten years, photonic nanostructures have represented a paradigm for the control of thermal radiations, offering a panel of exciting properties for energy applications [7]. In that context, we propose to study in the MIR range, the reflection / transmission / absorption properties of a polymer membrane, periodically structured with air holes. Indeed, we aim to demonstrate that depending on the geometrical parameters of the photonic membrane, we are able to modulate transmission / absorption coefficients in the wavelength range [7.5–11.5] µm which cover the maximum of the human body emissivity and then we study analytically the thermal effect of the membrane as a function of the geometrical parameters.

2. Design and simulation of a photonic polymer membrane

The theoretical calculations have been performed with the help of the Finite Element Method (FEM) as seen schematically Figure 1.

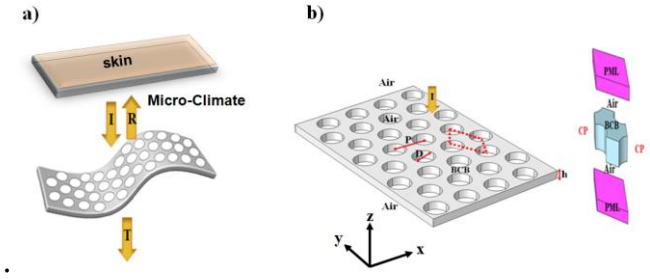

Figure 1: a) Principal scheme of the system with the direction of the incident (I), reflective (R) and transmitive (T) electromagnetic waves. b) (left) 3D view of the polymer membrane where h is the thickness, D the diameter and P the period. (Right) Elementary unit cell used for the FEM calculation with the absorbing (PML) and periodic (CP) boundary conditions.

3. Optical & thermal properties of the membrane

The Fig. 3a reports the evolution of the efficiency coefficient η for the reflection (black solid line), the transmission (blue solid line) and absorption (red solid line) as a function of the scaling factors α_i. and the figure 3b represent the temperature of the membrane BCB ,$\mathbf{T_{BCB}}$, as a function of the scaling factor α_i at different room temperature. Indeed, such homothetic variation of the parameters, following a scale law, induces a shift of the radiation effect of the membrane to the high wavelengths, thus emerging inside the human body emissivity.

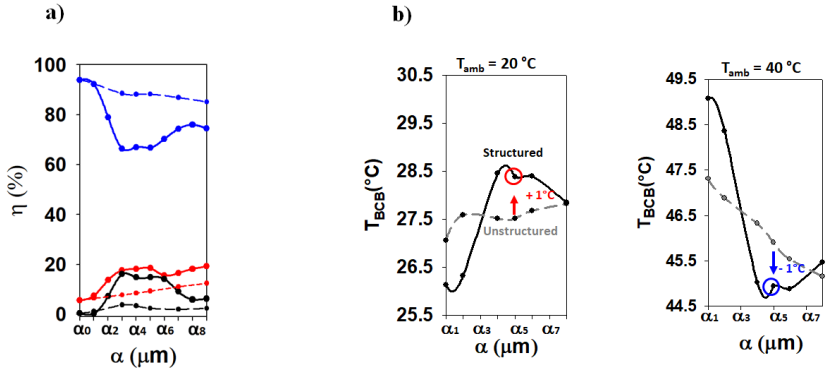

Figure 3:a)Evolution of the efficiency coefficient η, responses of the effective medium (dashed lines) and structured (solid lines) BCB membrane. b) Evolution of the membrane BCB temperature $\mathbf{T_{BCB}}$, as a function of the scaling factor α_i for a non-structured (grey lines) and structured (black lines) BCB membrane at different room temperatures

4. Conclusion

We have studied the optical and the thermal properties of the BCB memrane, showing the effect of the structure to control the reflection transmission and absorption spectra in the mid infrared. Also, the work is ongoing toward an experimental demonstration.

5. Acknowledgement

We thank Semi Lab for performing the refractive index measurement. S.A. thanks the society DAMART France for partial financial support of his PhD. This work was supported by the European Commission project Phototex under the INTERREG program France - Wallonie - Vlaanderen.

6. Reference

[1] K. J. Chua, S. K. Chou, W. M. Yang, and J. Yan, “Achieving better energy-efficient air conditioning – A review of technologies and strategies,” Appl. Energy, vol. 104, pp. 87–104, Apr. 2013.

[2] R. F. Rupp, N. G. Vásquez, and R. Lamberts, “A review of human thermal comfort in the built environment,” Energy Build., vol. 105, pp. 178–205, Oct. 2015.

[3] M. M. Yazdi and M. Sheikhzadeh, “Personal cooling garments: a review,” J. Text. Inst., vol. 105, no. 12, pp. 1231–1250, 2014.

[4] J. K. Tong, X. Huang, S. V. Boriskina, J. Loomis, Y. Xu, and G. Chen, “Infrared-Transparent Visible-Opaque Fabrics for Wearable Personal Thermal Management,” ACS Photonics, vol. 2, no. 6, pp. 769–778, Jun. 2015.

[5] P. B. Catrysse, A. Y. Song, and S. Fan, “Photonic Structure Textile Design for Localized Thermal Cooling Based on a Fiber Blending Scheme,” ACS Photonics, vol. 3, no. 12, pp. 2420–2426, Dec. 2016.

[6] P.-C. Hsu et al., “Radiative human body cooling by nanoporous polyethylene textile,” Science, vol. 353, no. 6303, pp. 1019–1023, Sep. 2016.

[7] Sawhney, A. P. S., Condon, B., Singh, K. V., Pang, S. S., Li, G., & Hui, D. (2008). Modern applications of nanotechnology in textiles. Textile Research Journal, 78(8), 731-739.

Matrix approach of Full-Field OCT for volumetric imaging of an opaque human cornea

Paul Balondrade[1], Victor Barolle[1], Laura A. Cobus[1], Kristina Irsch[2], Claude Boccara[1], Mathias Fink[1], and Alexandre Aubry[1]

[1]*Institut Langevin, ESPCI Paris, PSL University, CNRS UMR 7587, 1 rue Jussieu, 75005 Paris, France*
[2]*Institut de la Vision, CIC 1423, UPMC-Sorbonne Universities, UMR 968, INSERM U968, CNRS UMR 7210,Quinze-Vingts National Eye Hospital, France*

alexandre.aubry@espci.fr

Abstract: We report on a matrix approach of optical imaging that allows to overcome aberration and multiple scattering issues in microscopy. This allows in-depth diffraction-limited imaging of biological media over a wide field-of-view (FOV). © 2019 The Author(s)

OCIS codes: 110.0113, 290.4210, 010.1080.

1. Introduction

Optical microscopy offers the possibility to image biological tissue with a diffraction limited resolution ($\sim \mu$m). However, the heterogeneity of biological tissues can strongly affect light propagation at large depths by distorting the initial wavefront. Large and short range fluctuations of the refractive index can induce aberration and multiple scattering, respectively. Inspired by a recent work [1], we have developed a matrix approach to Full-Field Optical Coherence Tomography (FF-OCT) to push back the fundamental limit of aberrations and multiple scattering. Here, we report on the application of this approach to the imaging of the human cornea and the quantitative measurement of the corneal transparency.

2. Matrix approach

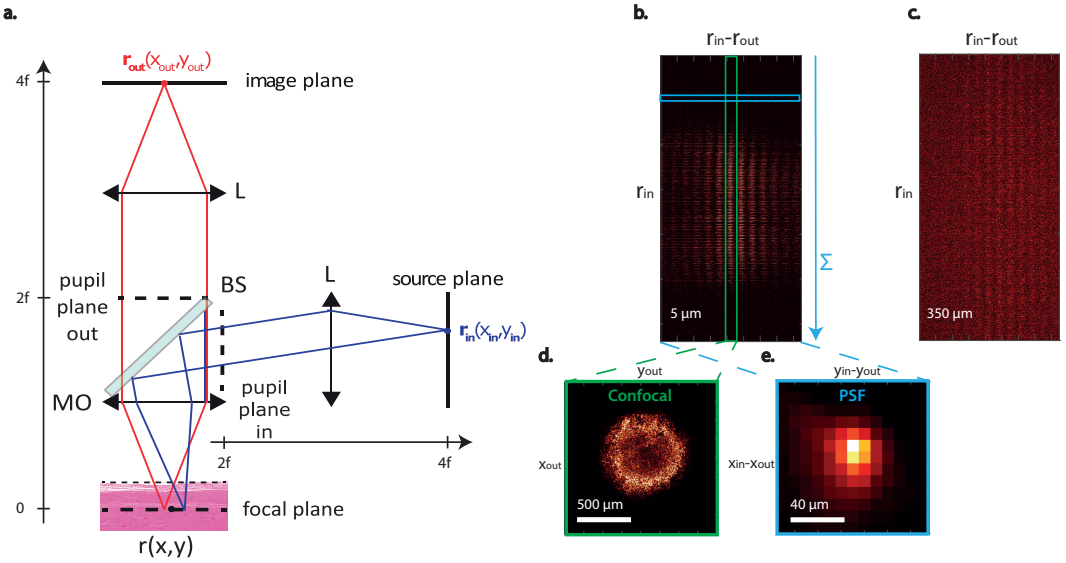

Fig. 1. **Matrix approach for FF-OCT a.** Imaging configuration for the measurement of the reflection matrix. **b**, **c.** The reflection matrix R($\mathbf{r_{out}} - \mathbf{r_{in}}$, $\mathbf{r_{in}}$) is shown for 5 μm and 350 μm depths in the cornea, respectively. **d.** *En-face* FF-OCT image corresponding to the confocal image where input and output focused points obey $\mathbf{r_{in}} = \mathbf{r_{out}}$. **e.** The focal spot averaged over all focal points $\mathbf{r_{in}}$.

The matrix approach for FF-OCT is based on the measurement of a time-gated reflection matrix **R** (Fig 1 b. and c.). Each column of **R** corresponds to the reflected wave-field in the image plane ($\mathbf{r_{out}}$) centered around the incident

focal point $\mathbf{r_{in}}$. The central column $R(\mathbf{r_{in}} = \mathbf{r_{out}})$ yields the confocal image of the sample in the focal plane (Fig 1 d.). Each line of $\mathbf{R}$ yields the point spread function (PSF) of the imaging system around each focal point of the FOV. The reflection matrix can be used to measure the amount of aberration that the incident wavefront has undergone inside the medium. At the surface of the cornea (Fig 1 b.), the majority of the energy is focused on the central column of the reflection matrix, meaning that spreading of the average focal spot (Fig 1 e.) is minimal at this depth (diffraction-limited focusing). Conversely, at larger depths (Fig 1 c.), the incident wave-field becomes distorted due to the cornea heterogeneities. By projecting $\mathbf{R}$ in the output pupil plane, the corresponding aberration phase law can be extracted. The application of its phase conjugate both at the input and output of $\mathbf{R}$ allows to compensate for aberrations and restore both the resolution and contrast of the image as if the cornea was transparent.

3. 3-D imaging of an opaque human cornea

We measured $\mathbf{R}(\mathbf{z})$ as a function of depth in an ex-vivo human cornea. As light propagates inside the cornea, it undergoes strong phase distorsion that severely degrades the quality of the FF-OCT image (Fig 2 b. and c.). This distorsion can be clearly observed on the spreading of the focal spot (Fig 2 d.). Conventional adaptive optics allows to correct for one part of the image but is not efficient over the whole FOV. Conversely, our matrix approach yields a high-quality image of the cornea over the whole FOV as if the inhomogeneities of the cornea had disappeared (Fig 2 f. and g.). Furthermore, the recovery of a diffraction limited PSF (Fig 2 h.) proves the success of the correction. This approach also allows a quantitative measurement of the scattering mean free path, l_s, inside the different layers of the cornea. This parameter is relevant to characterize corneal transparency, which can be impacted by several diseases such as keratoconus. Via a linear fit of the depth-dependent decrease of intensity (corrected for aberration effects), we measure an average l_s of 475 μm $\pm$ 25 μm in the stroma ((Fig 2 e.).

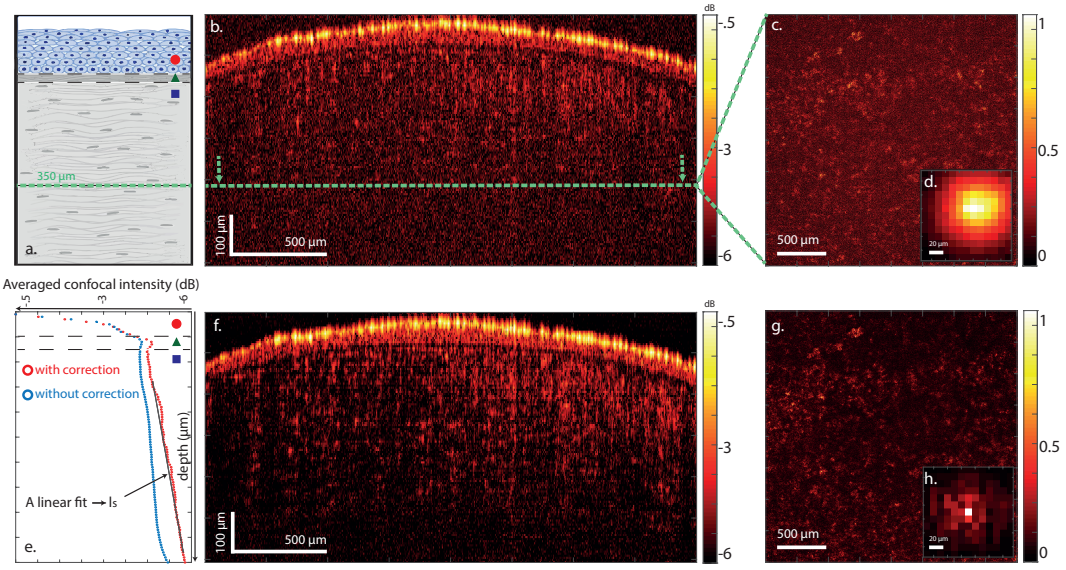

Fig. 2. **Aberration correction for imaging of a human cornea. a.** Scheme of the three first corneal layers. The red circle, green triangle and blue square respectively correspond to the epithelium, the Bowman's layer and the stroma. **b** Axial section of the FF-OCT image (in dB) of the cornea without and **f.** with correction for aberration. **c, g.** En-face FF-OCT image of the cornea at a depth of 350 μm before and after correction, respectively. **d, h.** Average focal spot deduced from $\mathbf{R}$ at the depth of 350 μm before and after correction, respectively. **e.** Average confocal intensity (in dB) versus depth inside the human cornea.

4. Conclusion and perspectives

The perspective of this work is to go beyond cornea and apply our approach to retinal and choroidal imaging. In addition, as this matrix approach is not limited to the study of the eye, future work will be applied to in-depth imaging of biological tissues.

References

1. A. Badon, D. Li, G. Lerosey, A. C. Boccara, M. Fink, A. Aubry "Smart optical coherence tomography for ultra-deep imaging through highly scattering media," Sci. Adv. **2**, e1600370 (2016).

Cross-correlation induced interference in the diffusely scattered light from combined surface and volume disorders

J.-P. Banon[1,2],* R. Pierrat[1], I. Simonsen[2,3], and R. Carminati[1]
[1] *Institut Langevin, ESPCI Paris, CNRS, PSL University, 1 rue Jussieu, 75005 Paris, France*
[2] *Surface du Verre et Interfaces, UMR 125 CNRS/Saint-Gobain, F-93303 Aubervilliers, France and*
[3] *Department of Physics, NTNU – Norwegian University of Science and Technology, NO-7491 Trondheim, Norway*
(Dated: September 29, 2019)

Interference patterns in the light diffusely scattered from combined randomly rough surfaces and volume dielectric fluctuations is studied by means of a single scattering theory. We show that, under certain conditions, exotic interference patterns can be induced by designing the cross-correlation between the surface and volume disorder.

I. INTRODUCTION

Complex media, either naturally occurring or man-made, may often exhibit fluctuations of refractive index in the bulk and surface roughness. These two sources of disorder lead to light scattering. In this work, we study the coupling between the scattering of light by surface and bulk disorder within a single scattering approximation. In the case of equal contribution of the two sources of disorder to the scattered power, we explore the effect of cross-correlation between surface and bulk disorder within two regimes. A regime in which the bulk out-of-plane correlation length is small compared with the thickness of the volume of dielectric fluctuations, which we refer to as the genuine volume regime, and a regime in which the bulk out-of-plane correlation length is large compared with the thickness of the volume of fluctuations, which we refer to as the surface-like regime or strong coupling regime. Only the latter is illustrated in this summary. A more complete study is given in Ref. [1].

II. SCATTERING SYSTEMS AND THEORY

The scattering system is composed of a homogeneous medium of dielectric constant ε_1 and a heterogeneous medium of average dielectric constant ε_2 and dielectric fluctuations $\Delta\varepsilon(\mathbf{r})$ bounded within a thickness L below the average surface. The two media are separated by a randomly rough surface of equation $x_3 = \zeta(x_1, x_2)$.

The surface profile function ζ and the dielectric fluctuation function $\Delta\varepsilon$ are given jointly as realizations of a continuous stationary Gaussian stochastic process. The cross-power spectral density of the surface profile and dielectric fluctuations is modelled by

$$\hat{W}_{\zeta\varepsilon}(\mathbf{p}, x_3) = \gamma(\mathbf{p})\, \hat{W}_{\zeta}^{1/2}(\mathbf{p}) \hat{W}_{\varepsilon}^{1/2}(\mathbf{p}, x_3)\,. \qquad (1)$$

Here $\hat{W}_\zeta$ and $\hat{W}_\varepsilon$ are respectively the surface and dielectric fluctuation power spectral densities. The function γ is the spectral cross-correlation modulator and is such that $|\gamma| \leq 1$ and $\gamma(-\mathbf{p}) = \gamma^*(\mathbf{p})$.

In the single scattering and scalar wave approximations, the total diffuse component of the average far-field intensity can be written as [2]

$$\langle I_{\text{tot}} \rangle_{\text{diff}} = \langle I_{\text{surface}} \rangle_{\text{diff}} + \langle I_{\text{correlation}} \rangle_{\text{diff}} + \langle I_{\text{volume}} \rangle_{\text{diff}}\,, \qquad (2)$$

where I_{surface} and I_{volume} are the intensity for the sole surface or volume disorder and $I_{\text{correlation}}$ is an interference term induced by the surface-volume cross-correlations and which can take positive and negative values. Each term in Eq. (2) is proportional to the corresponding power spectral density. In particular, the diffuse component of the cross-correlation term is proportional to the real part of cross-correlation modulator, $\langle I_{\text{correlation}} \rangle_{\text{diff}} \propto \Re(\gamma)$.

III. RESULTS AND DISCUSSION

Figure 1 illustrates three cases where interference patterns can be designed in the far-field. In all cases, the surface and dielectric fluctuation auto-correlation functions are Gaussian with identical in-plane correlation length. The out-of-plane dielectric correlation length is large compared with the slab thickness. The rms roughness and the slab thickness are sub-wavelength and the rms dielectric fluctuation is chosen such that the power scattered independently by the surface and by the volume are equal. For uncorrelated processes, the angular distribution of intensity would take the form of a bell shaped signal (not shown here). The three cases illustrated in Fig. 1 only differ by the spectral correlation modulator γ. In the first case, γ corresponds to a phase shift and interference fringes are induced in the intensity. The second and third cases correspond respectively to a phase shift bounded spectrally outside or inside a disk.

IV. CONCLUSION

We have demonstrated that in a single scattering regime, exotic interference patterns can be created in

* jean-philippe.banon@espci.fr

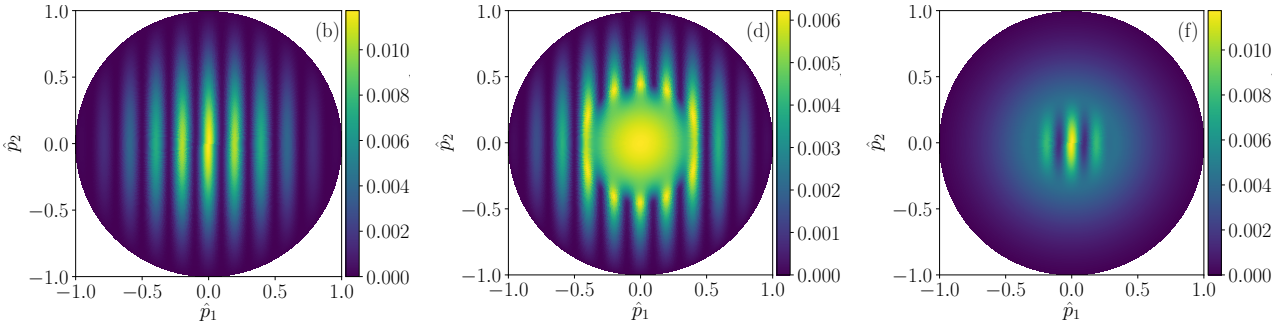

FIG. 1. Diffuse component of the MDRC in the **p**-plane (b,d,f). The surface and volume dielectric fluctuation have Gaussian correlation functions with in-plane correlation length $\ell_{\parallel} = \lambda/2$ and out-of-plane correlation length $\ell_{\varepsilon\perp} = 20\lambda$. The thickness of the slab supporting the dielectric fluctuation is $L = \lambda/20$. The rms roughness and rms dielectric fluctuation are chosen in such a way that the power scattered by the surface and volume independently are equal. (b) $\gamma(\mathbf{p}) = \gamma_0 \exp(i\,\mathbf{p}\cdot\mathbf{a})$ with $\mathbf{a} = 5\lambda\,\hat{\mathbf{e}}_1$. (d) $\gamma(\mathbf{p}) = \gamma_0 \exp(i\,\mathbf{p}\cdot\mathbf{a})\left[1 - \varphi(2|\,\mathbf{p}\,|/k_1)\right]$. (f) $\gamma(\mathbf{p}) = \gamma_0 \exp(i\,\mathbf{p}\cdot\mathbf{a})\,\varphi(2|\,\mathbf{p}\,|/k_1)$, with $\varphi(x) = \mathrm{H}(1-x^2)\exp(4 + 4/(x^2-1))$.

combined surface-volume disordered systems. The interference patterns are induced by modulating spectrally the cross-correlation between the two types of disorder. This is a simple example for which the splitting rule [3] for incoherent summation of the intensities of the two sub-systems for which only the surface is rough or the dielectric fluctuation are present fails. The present study can be of interest for disordered thin film characterization and design, and for background removal in interferometric scattering microscopy of nanoscale objects [4, 5].

[1] J.-P. Banon, I. Simonsen, and R. Carminati, Scattering of polarized light by weak correlated surface and volume disorders, To be submitted (2019).

[2] J. M. Elson, Phys. Rev. B **30**, 5460 (1984).

[3] A. Sentenac, H. Giovannini, and M. Saillard, J. Opt. Soc. Am. A **19**, 727 (2002).

[4] M. Piliarik and V. Sandoghdar, Nature Communications **5**, 4495 (2014).

[5] R. W. Taylor and V. Sandoghdar, Nano Letters **19**, 4827 (2019), pMID: 31314539.

Optimal Analog Multiplexing with Reconfigurable Wave-Chaotic Systems

P. del Hougne*, F. Mortessagne, O. Legrand, U. Kuhl
Institut de Physique de Nice, CNRS UMR 7010, Université Côte d'Azur, Nice, France
* philipp.delhougne@gmail.com

Résumé
We demonstrate how to optimally multiplex information from multiple incoming spatial degrees of freedom across multiple outgoing wave-front-shaping degrees of freedom. The latter correspond to single-port single-frequency measurements taken for a carefully tailored set of boundary configurations of a chaotic cavity, implemented with reflect-array metasurfaces. In our in-situ experiments, optimal boundary configurations improve the reconstruction fidelity by a factor of three. Our results are poised to impact computational microwave imaging.

1. Introduction

Coherent measurements across large apertures, as required for imaging, are notoriously challenging in the radio-frequency domain. Traditional solutions involving active or synthetic beamforming suffer from costly hardware and slow acquisition, respectively. An attractive solution which shifts this burden from the physical to the processing layer recently proposed to leverage the complexity (specifically, the frequency diversity) of media such as metamaterial apertures or chaotic cavities in order to multiplex the incoming spatial information across multiple single-port measurements, taken at independent frequencies [1], [2]. The initial information is then reconstructed in post-processing. For sparse incoming information, the reconstruction is even possible with an underdetermined set of such measurements using compressed-sensing techniques.

A refinement of this technique was then brought about by tunable complex media, paving the path toward single-port single-frequency operation. Tunable reflectarray metasurfaces placed inside a chaotic cavity provide substantial control over the wave field [3]. Randomly changing the configuration of such a metasurface completely changes the field, akin to changing the frequency by more than a correlation frequency. Hence incoming spatial information can also be multiplexed across measurements taken for different random metasurface configurations at a single port and a single frequency [4].

Here, we explore how to make the best out of the control offered by tunable metasurfaces. We show with an in-situ experimental demonstration that a carefully tailored set of metasurface configurations significantly improves the reconstruction fidelity of the incoming information as compared to the thus far employed random configurations. Specifically, in our experiment the reconstruction fidelity is at least tripled for the same number of measurements taken. Using random configurations, similar performance could only be achieved with much more measurements. Yet limiting the number of necessary measurements is desirable to improve a wide range of metrices, including acquisition time, power consumption and processing burden.

2. Experiment and Results

Our in-situ experimental setup and some preliminary results are shown in Fig. 1. In (b) and (c) we contrast the distribution of eigenvalues before any optimization and after optimizing either diversity or path loss of the channel matrix. The corresponding reconstruction fidelities are plotted in (d). While purely minimizing path loss is seen to deteriorate the performance by only strengthening the strongest eigenvalue, maximizing channel diversity boosts the reconstruction

quality by a factor of three in our experiment.

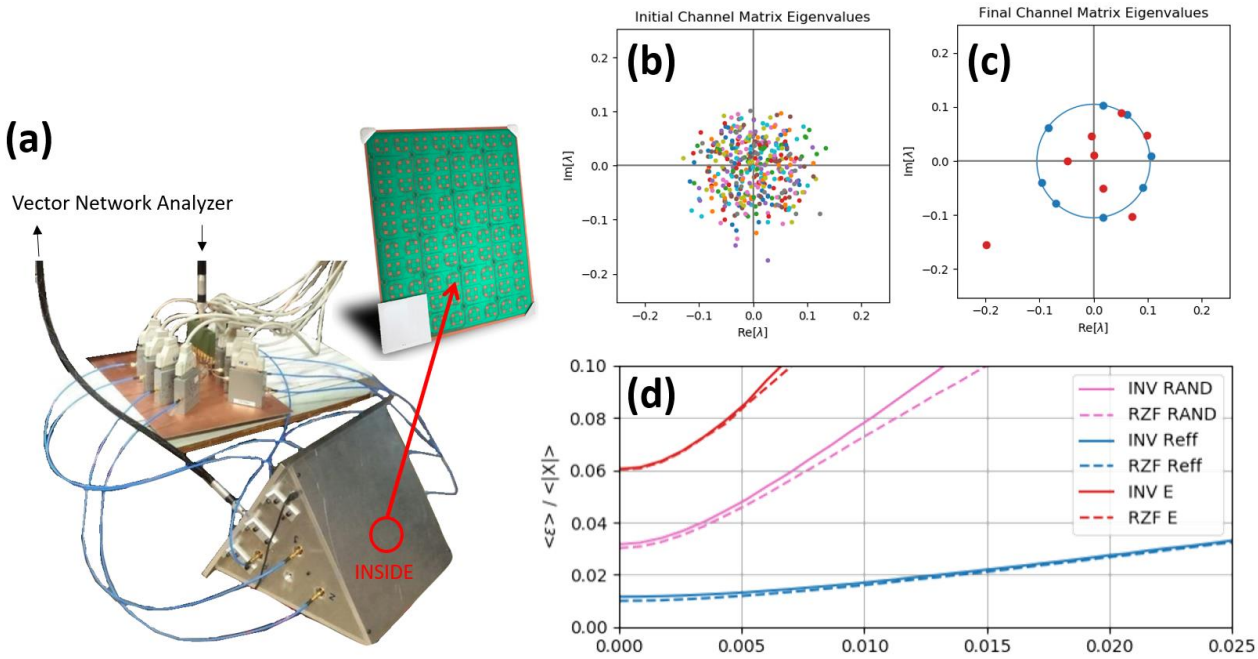

Figure 1. (a) Experimental setup, the inset shows the reflect-array metasurface; (b) distribution of eigenvalues for random sets of boundary conditions; (c) eigenvalues after optimizing channel diversity (blue) or path loss (red); (d) normalized reconstruction error as function of normalized SNR for random (pink) sets of configurations and the two optimizations shown in (c).

4. Conclusion

For information multiplexing from spatial to wave-front shaping degrees of freedom, using tailored configurations substantially improves the channel matrix properties and reconstruction quality (in our experiments at least by a factor of three). It does not bring about any additional cost for hardware or during operation, only a one-off calibration step is necessary.

5. Remerciements

The authors are supported by the French “Agence Nationale de la Recherche” under reference ANR-17-ASTR-0017. The metasurface prototype was purchased from Greenerwave.

The project was initiated, conceptualized, conducted and written up by P.d.H. Funds were acquired by F.M, O.L. and U.K. All authors thoroughly discussed the results.

6. Bibliographie

[1] J. Hunt *et al.*, “Metamaterial Apertures for Computational Imaging,” *Science*, vol. 339, no. 6117, pp. 310–313, Jan. 2013.

[2] T. Fromenteze *et al.*, “Computational imaging using a mode-mixing cavity at microwave frequencies,” *Appl. Phys. Lett.*, vol. 106, no. 19, p. 194104, May 2015.

[3] M. Dupré, P. del Hougne, M. Fink, F. Lemoult, and G. Lerosey, “Wave-Field Shaping in Cavities: Waves Trapped in a Box with Controllable Boundaries,” *Phys. Rev. Lett.*, vol. 115, no. 1, p. 017701, Jul. 2015.

[4] T. Sleasman, M. F. Imani, J. N. Gollub, and D. R. Smith, “Microwave Imaging Using a Disordered Cavity with a Dynamically Tunable Impedance Surface,” *Phys. Rev. Applied*, vol. 6, no. 5, p. 054019, Nov. 2016.

Compressed three-dimensional super-resolution imaging with speckles

M. Pascucci[1], S. Ganesan[1], A. Tripathi[2], O. Katz[2], V. Emiliani[1] and Marc Guillon[1]
[1] : *Neurophotonics laboratory, CNRS UMR8250, 45 rue des Saints Pères, 75006 Paris*
[2] : *Department of Applied Physics, The Hebrew University of Jerusalem, Jerusalem 9190401, Israël*
[3] : *Université de Paris, CNRS, SPPIN – Saints-Pères Paris Institute for the Neurosciences, 45 rue des Saints-Pères, 75006 Paris*
marc.guillon@parisdescartes.fr

Résumé
This work relates the use of speckle patterns to achieve efficient 3D super-resolution microscopy by optical saturation by compressed sensing. 3D imaging is achieved by a 2D scan of the sample only. Super-resolution is made possible thanks to the high density of intrisic optical vortices in speckles. Optical vortices are indeed associated with intensity minima allowing fluorescence confinement to sub-diffraction dimensions.

1. Introduction

Fluorescence microscopy has proven to be a fundamental tool for biology. Two main important parameters to optimize are resolution improvement - down to nanometric scales - and fast 3D imaging. However, optimized super-resolution imaging requires collecting fluorescence signal up to the organic probe exhaustion. This requirement has been proven to be hardly compatible with 3D imaging since most of optical designs imply fluorescence excitation in out-of-focus planes. This signal is then induced to be wasted by numerical or physical optical sectioning. Furthermore, due to Brownian motion, imaging of nano-objects demands especially fast 3D techniques.

2. Imaging with speckles

Random light patterns feature two main properties that make them ideally suited for fast 3D super-resolution microscopy. First, speckle patterns lying in different transverse planes are orthogonal relatively to the cross-correlation product. This property exactly provides the random-projection-measurement configuration, optimal for achieving *compressed imaging reconstruction* [1]. Second, speckles naturally contain a high spatial density of *optical vortices* such as those typically used in super-resolution STED microscopy [2], making them suitable to confine fluorescence to sub-diffraction dimensions [3].

3. Typical result

An illustration of the principle of the imaging technique as well as typicial results obtained is shown in Fig. 1.

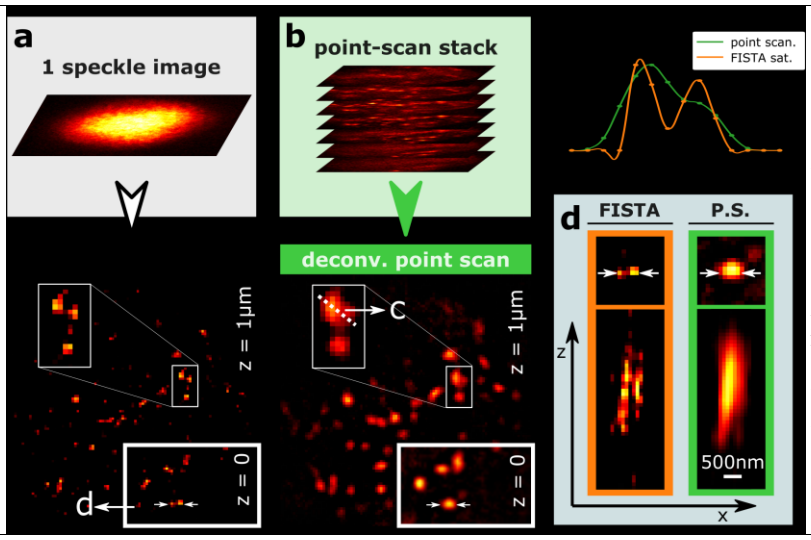

Fig. 1: A single 2D speckle image allows 3D imaging by FISTA [4] (a) while 3D scanning is typically required by classical microscopy (b). Saturated excitation conditions further provides super-resolution both in the transverses (c) and along the axial (d) directions.

4. Conclusion

Here, we demonstrate 3D super-resolution imaging by a single 2D speckle-scan under saturated excitation conditions [4]. Reconstruction is achieved by a compressed sensing algorithm (FISTA [5]) that takes into account the sample sparsity and makes use of every collected fluorescence photons.

5. Remerciements

This work was supported by grants from the Région Ile-de-France (PhD program) and the French-Israeli Laboratory ImagiNano.

6. Bibliographie

[1] D. L. Donoho, IEEE Transactions on Information Theory **52,** 1289-1306 (2006)
[2] K.I. Willig, R.R. Kellner, R. Medda, B. Hein, S. Jakobs, and S.W. Hell, Nat. Methods **3,** 721-723 (2006).
[3] M. Pascucci, G. Tessier, V. Emiliani, M. Guillon, Phys. Rev. Lett. **116,** 093904 (2016).
[4] M. Pascucci, S. Ganesan, A. Tripathi, O. Katz, V. Emiliani, and M. Guillon. Nat. Commun. **10,** 1327 (2019)
[5] A. Beck and M. Teboulle, SIAM Journal on Imaging Sciences 2, 183-202 (2009).

Narrow spectral filtering detection techniques for Ultrasound Optical Tomography of biological tissues with a Tm:YAG crystal submitted to a weak magnetic field

C. Venet[1,3] , J.-P. Huignard[1], F. Ramaz[1], T. Chanelière[2], A. Louchet-Chauvet[3]
[1] : *Institut Langevin ESPCI Paris, CNRS UMR7587, 1 rue Jussieu 75005 Paris,*
[2] : *Institut Néel, CNRS/UGA UPR2940, 25 av. des Martyrs 38000 Grenoble*
[3]: *Laboratoire Aimé Cotton, CNRS UMR9188, Bât. 505 Campus d'Orsay 91405 Orsay*
Email : caroline.venet@espci.fr

Résumé
The combination of Light and Ultrasound (US) via the acousto-optic effect can be used to image deep into biological tissues, where classical imaging is prohibited due to multiple scattering processes. We have developed a long-lived narrow filter@793nm ($\delta\lambda=10^{-6}$nm) using the spectral holeburning effect encountered with a rare-earth doped crystal under a weak magnetic field, in order to filter the photons tagged by the US, who bring the information of a local optical contrast due to the ballistic propagation of an acoustic wave within these media.

1. Introduction

Ultrasound Optical Tomography (UOT) is a hybrid technique combining Light and Ultrasound (US) to image deep into highly scattering media, e.g. biological tissues. Indeed, it allows to measure optical contrast guided by the US, which remain ballistic beneath 20MHz in tissues. Up to now, most of the techniques used to detect photons tagged by the US (i.e. shifted from the US frequency) are based on interferometric detections (two-waves mixing in photosensitive media, e.g. photorefractive crystals, digital holography), thus sensitive to speckle decorrelation time of living tissue due to e.g. blood flow, which degrades the contrast of the photo-induced hologram.

We have recently developed a new architecture that discriminates the flux of the photons tagged by the US using a rare earth doped crystal at cryogenic temperature (T=3K). Since an optical flux is recorded, such a technique is intrinsically immune to phase variations linked to in vivo experiment, e.g. blood circulation, Brownian motion; to achieve this, we create an ultra-narrow transparency window of typically some MHz (absorption hole) within the inhomogeneous absorption line of Tm^{3+}:YAG@793nm using the Spectral HoleBurning effect (SHB). This way, the huge background of the carrier (laser frequency) transmitted by the sample is blocked by the crystal and one measures essentially the flux of the tagged-photons. The choice of Tm:YAG is motivated by the existence of a narrow absorption line@793nm (width ~ 20GHz) within the optical therapeutic window (650-1100nm), where absorption of biological markers (e.g, blood) is reduced. The hole lifetime is an important parameter affecting detection efficiency, because it favors the hole-depth, and thus the transparency of the crystal for the photons that have crossed the ultrasonic field (tagged-photons are shifted of the US-frequency from the carrier). In a sequence of data acquisition, it is necessary to prepare the crystal in burning a hole with a pump beam prior to the US excitation, then shut this excitation during the imaging step in order to avoid a strong background onto the detector (avalanche photodiode), which can be blurred. As shown in Fig.1, the intrinsic hole dynamics comes from a metastable level ($^3F_4$) which relaxes to the ground state in approximately 10ms. Some early UOT results have been obtained with this configuration [1], and proved the potential of the technique. However, this lifetime can be enhanced with the application of a weak magnetic field (typically 200G), yielding a hyperfine Zeeman splitting

within the Tm ground-state (also in the excited ones). As a consequence, the relaxation-time between these levels increases, leading to a hole lifetime of some 35s.

As indicated in Fig.1c, the Zeeman coefficient in the ground-state is 285MHz/T yielding a splitting of ~6MHz between the sublevels with a magnetic field of 200G (20mT). But in order to benefit from this longer lifetime, such a splitting requires a narrow linewidth laser, and for this purpose we have performed a stabilization loop with a stabilized Fabry-Perot cavity.

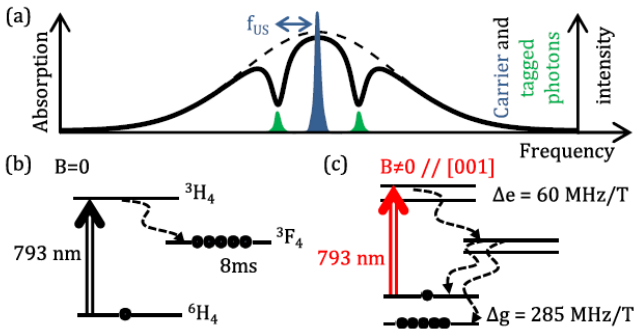

Fig.1: Holeburning mechanisms in Tm^{3+}:YAG@793nm without (b) and with (c) magnetic field.

As a proof of principle of the method, we have performed 2D-images of a millimetric absorbing inclusion embedded within a scattering phantom, with and without the magnetic field (230G), using a single acoustic transducer working at 5MHz in a burst regime (Fig.2). Both images have been performed with the same averaging of US shots (x100), and it appears effectively that the application of the magnetic field enhances noticeably the contrast-to-noise ratio of the signal, from a factor of 1 to 32, with an acquisition time reduced by a factor of about 16.

Fig.2: UOT images of an absorbing inclusion using spectral holeburning filtering in Tm:YAG, in the presence of a weak magnetic field (right), and without (left). An axial profile along the US propagation is plotted for comparison.

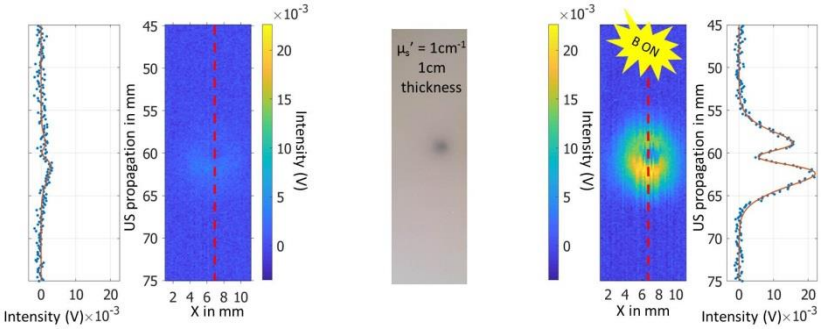

Conclusions

We have shown that UOT techniques using the spectral holeburning effect can be significantly improved in applying a weak magnetic field on a crystal of Tm:YAG for it increases the holelifetime from 10ms to 35s if using a stabilized laser. Next step will consist in performing images with an ultrasound imaging device and apply it in vivo, and also lock our laser on the spectral hole itself.

References

[1] Y. Li, H. Zhang, C. Kim, K. H. Wagner, P. Hemmer, and L. V. Wang, "Pulsed ultrasound-modulated optical tomography using spectral-hole burning as a narrowband spectral filter", Appl. Phys. Lett. 93, 11111 (2008).

[2] C. Venet, M. Bocoum, J.-B. Laudereau, T. Chaneliere, F. Ramaz, and A. Louchet-Chauvet, "Ultrasound-modulated optical tomography in scattering media: flux filtering based on persistent spectral hole burning in the optical diagnosis window," Opt. Lett. 43, 3993-3996 (2018).

Collective modes of hyperuniform resonant media

Romain Monsarrat[1], Rémi Carminati[1],Arnaud Tourin[1],
Romain Pierrat[1], Arthur Goetschy[1]

[1] Institut Langevin, ESPCI Paris, PSL University, CNRS, Paris, France
romain.monsarrat@espci.psl.eu
arthur.goetschy@espci.psl.eu

We present a preliminary analysis of the relation between macroscopic properties such as waves transport regimes, and the microscopic properties of the modes in a disordered medium. Our system consists in a set of highly resonant dipoles, spatially correlated in a hyperuniform pattern. The transport properties are inferred using analytical models for the scattering cross-section and the mean free path. Systems in different transport regimes were simulated numerically through the coupled dipoles method, giving access to the statistical properties of the distribution of modes. We analysed the influence of spatial correlations on the spectrum for both scalar and vector waves and in particular localisation effects apparently related to a polaritonic-like gap which disappears in the case of vector waves.

The objective of this project is to fill the gap between the study of fully disordered systems [1] and the physics of order and photonic crystals. In the last decade, the group of Torquato [2] came up with a certain type of correlated media called hyperuniform, where there is a continuous variable to describe the degree of correlation χ. These structures are defined by their structure factor which is mostly the norm of the Fourier transform of the spatial distribution. Fully disordered systems (Poissonian distributed) correspond to the case $\chi = 0$. There is a subtlety in the case of photonic crystals since different lattices correspond to different maximum values of χ but crystals appears usually around 0.8. An example of a hyperuniform distribution is shown in figure 1.

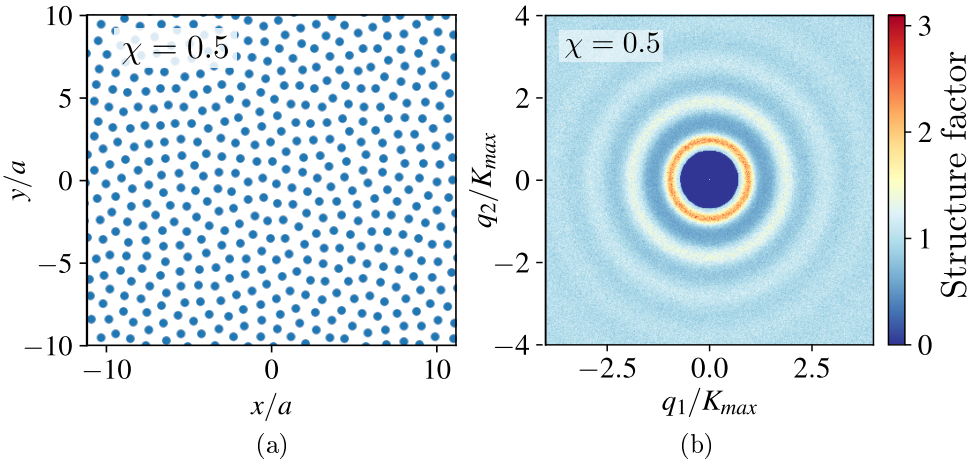

Figure 1: (a) - Spatial distribution of a 2D Stealthy HyperUniform pattern (SHU). (b) - Structure factor of the distribution displayed in (a). The zero structure factor for low $\mathbf{q}$ expresses a long range spatial order, but the series of rings at intermediate $\mathbf{q}$ and the pattern on figure (a) indicates short range correlations.

Macroscopic transport properties such as the effective index or the mean free path are usually complicated to compute analytically for a correlated system. These properties can nevertheless be accessed using the distribution of the modes in the medium. Since the system consists of point-like resonant dipoles in an open media, the coupled dipoles approach gives access to the full spectrum, in particular the detuning from the bare resonance $(\omega_n - \omega_0)/\Gamma_0/2$ and the linewidth Γ_n/Γ_0. The spatial shape of the modes can also be obtained and be aggregated into a simpler observable called the Inverse Participation Ration (IPR) which describes the spatial degree of localisation.

The main finding of this work is that spatial correlations tend to shift the different transport regimes toward lower densities [3]. This result holds for both scalar and vector fields. Figure 2 shows the transition from (a) a fully disordered system in the diffusive regime toward (b) a partially effective medium at high χ in the case of vector waves. Indeed, the rosary of spots in (b) for positive detuning is characteristic of the effective regime where each patch accounts for a geometrical resonance of the sphere.

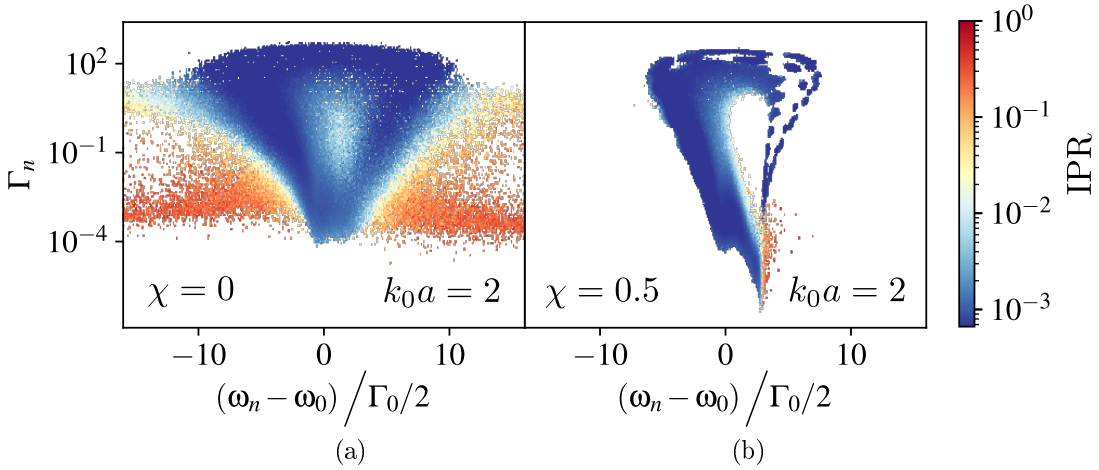

(a) (b)

Figure 2: Distribution of the quasi-modes of a set of resonant dipoles in a sphere, coupled with the dyadic Green function accounting for the vector nature of waves in the uncorrelated case (a) and where half of the degrees of freedom have been imposed (b). The colormap expresses the spatial degree of localisation of each individual mode: red for highly localised on a few scatterers and blue for a collective mode.

References

[1] A. Goetschy and S. E. Skipetrov, *Phys. Rev. E* **84**, 011150 (2011).

[2] S. Torquato, G. Zhang, and F. H. Stillinger, *Phys. Rev. X* **5**, 021020 (2015).

[3] O. Leseur, R. Pierrat, and R. Carminati, *Optica* **3**, 763–767 (2016).

Fluorescence Speckle Correlation Spectroscopy

Anirban Sarkar[1], Irène Wang[1], Jörg Enderlein[2], Jacques Derouard[1], Antoine Delon[1,*]
[1] : *Univ. Grenoble Alpes, CNRS, LIPHY, F-38000 Grenoble, France*
[2] : *Third Institute of Physics-Biophysics, Georg August University, 37077 Göttingen, Germany*

**Email: antoine.delon@univ-grenoble-alpes.fr*

Résumé
Here, we present a new modality to find the diffusion constant of 2D motion of particles, hidden behind a scattering layer, through speckle cross-correlation. We compare the results with that of single particle tracking method.

1. Introduction

Fluorescence correlation spectroscopy is used extensively for quantitative characterization of biomolecules at very low concentration. However, light aberration and scattering from the tissues are two major factors that affect the results strongly. Although adaptive optics arrangement can correct the aberrations of light to some extent, it fails completely to eliminate the light scattering effect. Recently, exploiting the fact that autocorrelation of a speckle pattern is a sharply peaked point spread function and the optical memory effect, non-invasive imaging of fluorescent sample has been possible [1–3]. In this study, we employ a modality based on speckle correlation enabled via optical memory effect to study 2D diffusion of fluorescent sample hidden behind a scattering film.

2. Experiments and results

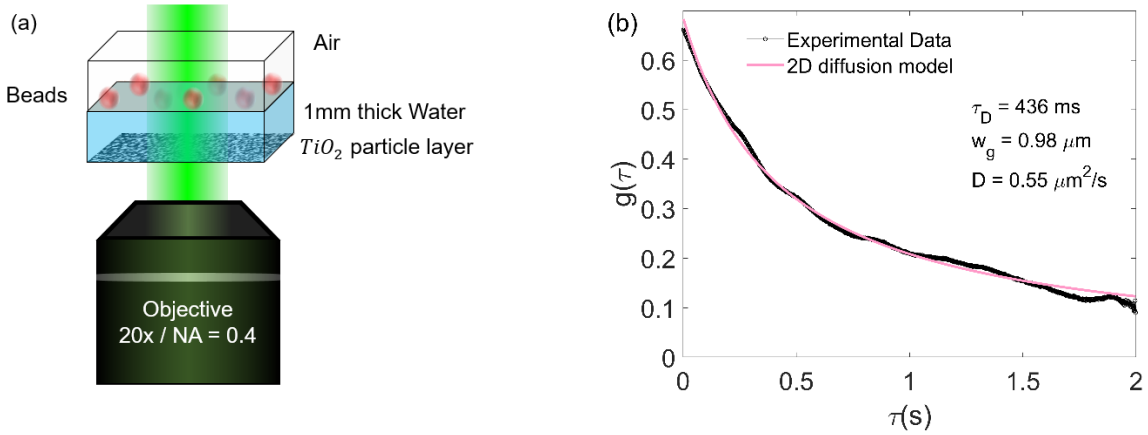

Fig. 1: (a) Schematic of the experiment (shown in part). (b) Temporal image cross-correlation acquired from a single bead fluorescence speckle is plotted with delay.

We realized a 2D diffusing model system by confining fluorescent polystyrene beads of 1µm diameter at the water/air interface behind a TiO_2 diffuser. Beads were excited by speckle illumination and the emission speckle was detected in an epi-fluorescence configuration. 2D diffusion constant obtained by temporal image cross-correlations of a single bead emission speckle is compared with that obtained by single particle tracking without the scattering layer.

Diffusion constant of the polystyrene particle obtained by speckle cross-correlation method is $D = 0.55\ \mu m^2/s$, which is quite close to that obtained by single particle tracking and the theoretical value.

4. Conclusion

In conclusion, in this study, we have presented a new method in the form of speckle image correlations to obtain the 2D diffusion constant of a particle hidden behind a scattering layer. Quantitative agreement between the results obtained by the speckle correlation and single particle tracking technique establishes the potential application of this technique in correlation spectroscopy. Superimposed multiple beads speckle patterns were also studied and the results will be presented at the meeting.

6. Bibliographie

[1] J. Bertolotti et al, Nature **491**, 232-234 (2012)
[2] O. Katz et al, Nat. Photonics **8**, 784-790 (2014)
[3] M. Hofer et al, Opt. Express **26**, 9866-9876 (2018)

Absorption of light in correlated disordered media

A.S. Sheremet[1], R. Pierrat[1], R. Carminati[1]
[1] : *Institut Langevin, ESPCI Paris, PSL University, CNRS*
1 rue Jussieu, 75005 Paris, France
Alexandra.sheremet@espci.fr

Abstract

Light absorption in complex disordered materials is substantially influenced by spatial correlations (partial order). We setup a multiple scattering theory to compute the average absorbed power, and to study the impact of spatial correlations. The results should pave the way towards the engineering of nanostructured blackbody-like disordered materials.

The study of wave propagation in disordered media has revealed a range of fascinating phenomena, from the emergence of mesoscopic intensity correlations to Anderson localization. The enhancement of light absorption in multiple scattering materials has attracted increasing attention. Interestingly, it has been shown that engineering the level of partial order (through spatial correlations) has a substantial effect in the absorbed power [1].

In this work, we consider scattering and absorbing correlated particles. We derive an exact equation for the statistically averaged absorption power applying a diagrammatic approach similar to that used in [2]. Using this model, we show that hyperuniform materials have the optimum disorder structure to achieve the maximum of the absorption power. Moreover, we show that the absorption mean-free path weakly depends on the structural correlations. These results can help guiding the design of nanostructured materials with an engineered degree of disorder, and showing broadband absorption over a large angular range.

Acknowledgments

This work is supported by LABEX WIFI (Laboratory of Excellence within the French Program “Investments for the Future”) under references ANR-10-LABX-24 and ANR-10-IDEX-0001-02 PSL.

References

[1] F. Bigourdan, R. Pierrat, and R. Carminati, Enhanced absorption of waves in stealth hyperuniform disordered media, *Optics Express* **27**, 8666 (2019).
[2] R. Pierrat, R. Carminati, and J.-L. Le Gouët, Photon echoes in strongly scattering media: A diagrammatic approach, *Phys. Rev. A* **97,** *063816 (2018)*.
[3] A.S. Sheremet, R. Pierrat, and R. Carminati, Optimizing light absorption in correlated disordered media: A diagrammatic approach, *in preparation* (2019).
[4] O. Leseur, R. Pierrat, and R. Carminati, High-density hyperuniform materials can be transparent, *Optica* **3**, 763-767 (2016).

Matrice de Réflexion Acousto-Optique

Louis Dutheil[1], Maïmouna Bocoum[1], Sébastien Popoff[1], François Ramaz[1]
[1] *ESPCI, PSL Research University, CNRS UMR 7587, Institut Langevin, 1 rue Jussieu, 75005 Paris*

Résumé

L'imagerie acousto-optique permet de sonder le contraste optique de milieux biologiques à des profondeurs où la microscopie échoue en raison de la diffusion de la lumière par les inhomogénéités. Cependant, la résolution de l'imagerie est limitée par la longueur d'onde des ultrasons, plusieurs ordres de grandeur plus grande que la limite de résolution en microscopie optique. En utilisant les techniques de modulation du front d'onde, nous proposons de mesurer les matrices de réflexion acousto-optiques, qui lient le champ optique incident au champ rétrodiffusé des photons marqués par les ultrasons dans un milieu diffusant. L'acquisition de plusieurs matrices en déplaçant l'excitation ultrasonore permettra de remonter à une information sur des variations spatiales plus petites que la longueur d'onde acoustique, permettant ainsi d'améliorer la résolution d'imagerie pour s'approcher de la limite de diffraction optique.

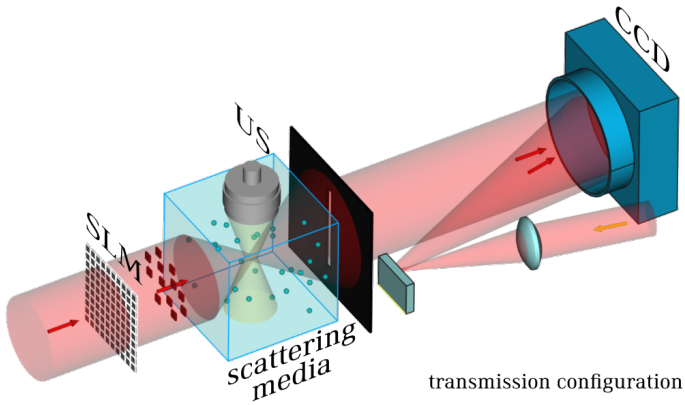

transmission configuration

Institut Langevin
ONDES ET IMAGES

ESPCI PARIS | PSL

cnrs